Electronic Supplementary Information

Reducing hole-injection hurdles of OER electrocatalysts derived from Ru doped FeNi metal–organic framework anchored with FeOOH

Chih-Hung Chou[a], Chen-Hao Yeh[b], Pei-Lun Chen[a], Kuan-Han Lin[a], Chia-Ying Wu[b], Zhi-Cheng Yan[a], Po-Hsuan Hsiao[1], and Chia-Yun Chen[a,c,d*]

[a]Department of Materials Science and Engineering, National Cheng-Kung University, Tainan 701, Taiwan

[b]Department of Materials Science and Engineering, Feng Chia University, Tainan 407102, Taiwan

[c]Program on Semiconductor Packaging and Testing, Academy of Innovative Semiconductor and Sustainable Manufacturing, National Cheng Kung University, Tainan 70101, Taiwan

[d]Hierarchical Green-Energy Materials (Hi-GEM) Research Center, National Cheng Kung University, No.1 University Road, Tainan 701, Taiwan

*Email: timcychen@mail.ncku.edu.tw

S1 Morphological and elemental compositions of Ni MOFs and FeNi MOFs

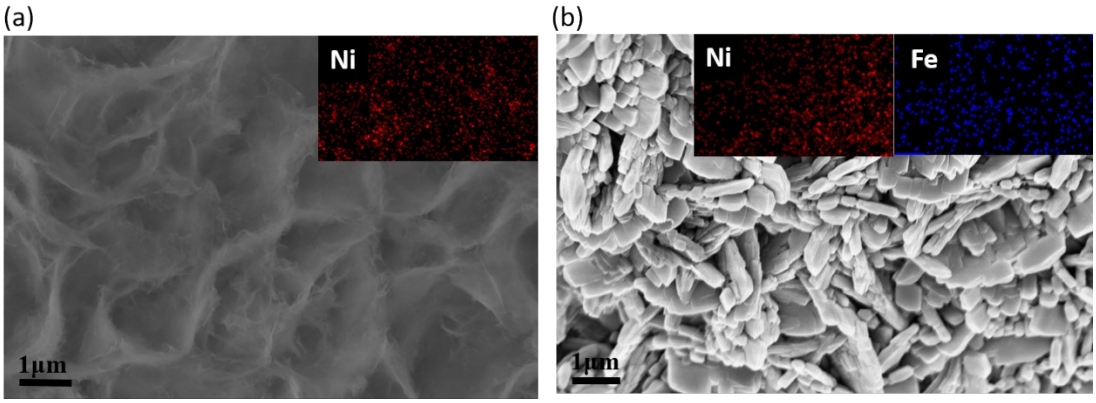

Fig. S1 Top-view SEM images of (a) Ni MOFs and (b) FeNi MOFs synthesized with one-pot precipitation processes. The inset figures show the correlated EDS mapping results, indicating the uniform formation of Ni MOFs and FeNI MOFs, respectively.

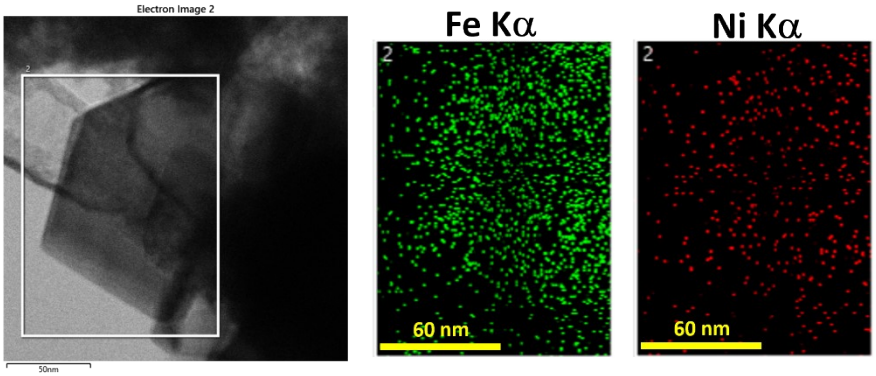

Fig. S2 Representative TEM image and correlated elemental EDS mappings of staggered FeNi MOFs, showing the uniform distributions of Fe and Ni constitutes, respectively.

S2 XPS examinations of Ni MOFs and FeNi MOFs

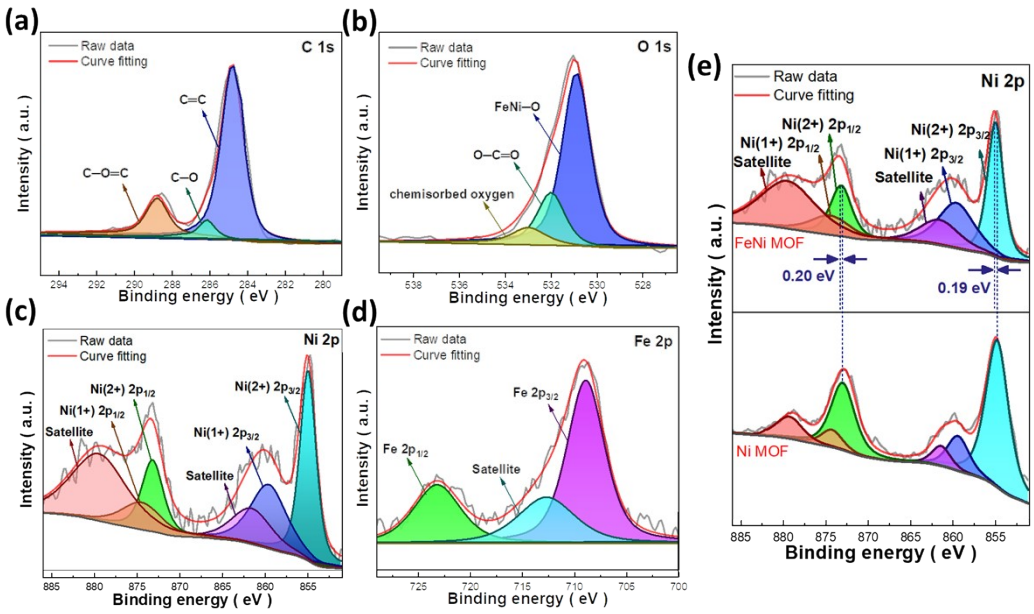

Fig. S3 Spectral examinations of (a) C 1s (b) O 1s (c) Ni 2p (d) Fe 2p in XPS spectra obtained from FeNi MOFs. (e) Spectral comparison of Ni 2p signatures from FeNi MOFs and Ni MOFs, indicating the explicit blue shift of correlated Ni 2p patterns.

The elemental compositions and chemical features of various MOF structures are investigated, as shown in Fig. S3. In C 1s spectrum, three distinct peaks are observed, corresponding to C=C (284.8 eV), C-O (286.2 eV), and C-O=C (288.8 eV), respectively, which are attributed to the presence of benzene rings and terephthalic linkers, as presented in Fig. S3(a). In O 1s spectrum, the bonding features of benzene rings and carboxylic groups can be observed at 530.8 eV and 532.0 eV, respectively,

as shown in Fig. S3(b). In Ni 2p spectrum [Fig. S3(c)], the Ni (2+) signatures are observed at 855.0 eV and 873.2 eV, and the Ni (1+) bonds are spectrally located at 859.6 eV and 874.5 eV. In Fe 2p spectrum [Fig. S3(d)], the spectral patterns of Fe $2p_{1/2}$ and Fe $2p_{3/2}$ are observed at 709.0 eV and 722.6 eV, respectively. By comparing the spectral features of Ni 2p from FeNi MOFs and Ni MOFs, the explicit blue shifts of correlated Ni 2p patterns in FeNi MOF relative to those of Ni MOFs are evidenced, as denoted in Fig. S3(e).

S3 Compositional analyses of FeNi MOFs and three various Ru-doped FeNi MOFs

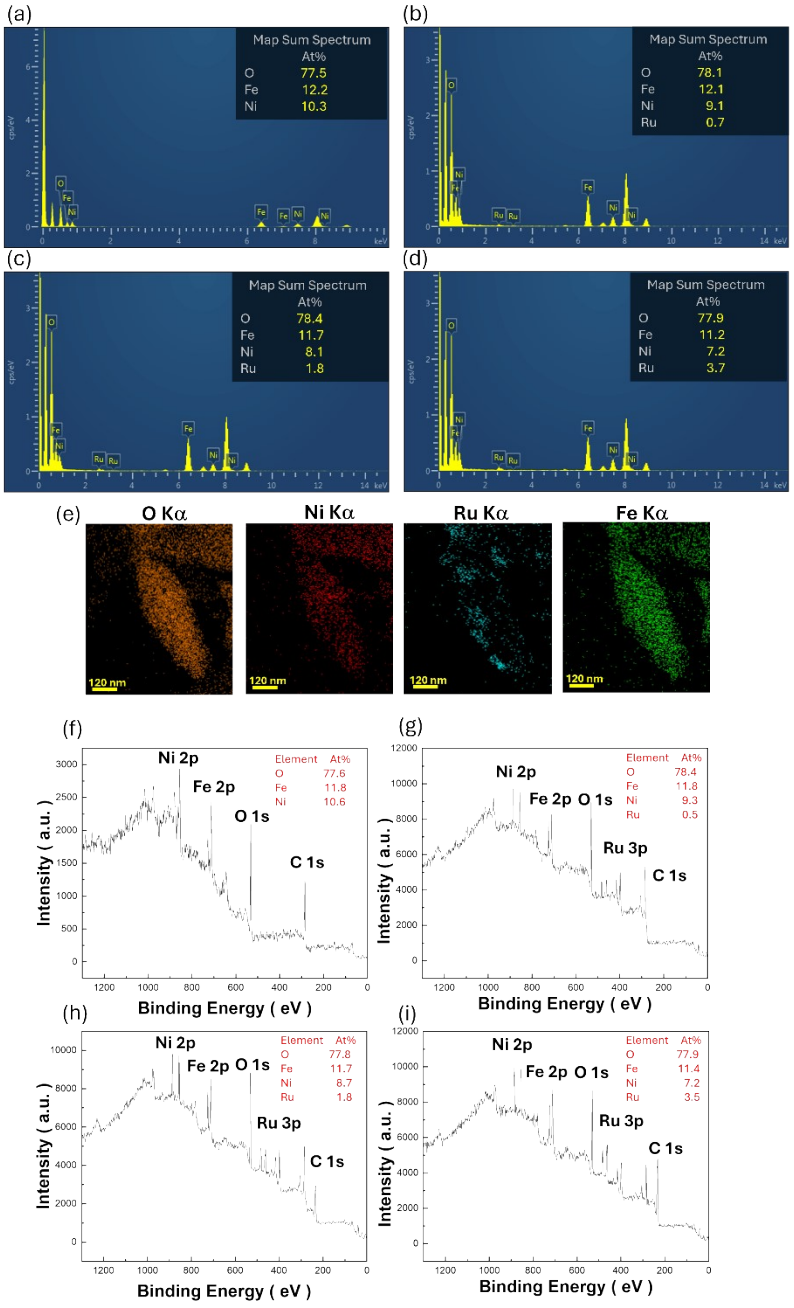

Fig. S4 Elemental characterizations of EDS spectra and correlated semi-quantitative results: (a) Bare FeNi MOFs and Ru-doped FeNi MOFs prepared with three various $RuCl_3$ concentrations, including (b) 1 mM, (c) 2 mM and (d) 4 mM, respectively. The Ru contents are found from 0.7 at% (Fig. S4(b)), 1.8 at% (Fig. S4(c)) to 3.7 at% (Fig. S4(d)). In addition, the representative EDS mappings of Ru-doped FeNi MOFs (2 mM) are displayed in Fig. S4(e). Quantitative XPS analyses of the relevant samples are presented in Figure S4(f)-4(i), where the elemental compositions are roughly corresponded to the results of EDS analyses, respectively, indicating the constitutional difference of four samples tested in this work.

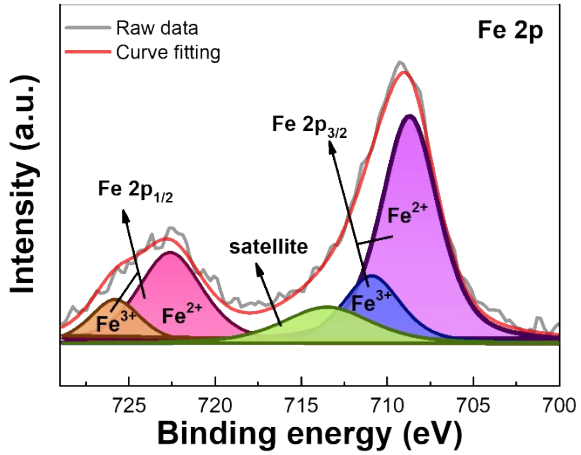

Fig. S5 XPS Fe 2p spectrum of Ru-doped FeNi MOFs. The co-existence of Fe^{2+} (at 708.6 eV and 722.7 eV correspond to $2p_{3/2}$ and $2p_{1/2}$, respectively) and Fe^{3+} signals Fe^{3+} (at 710.8 eV and 725.7 eV corresponding to $2p_{3/2}$ and $2p_{1/2}$, respectively) is demonstrated. In addition, the XPS intensity ratio of Fe $2p_{1/2}$ in viewing I_{Fe3+}/I_{Fe2+} is around 0.4.

S4 DFT calculation for unveiling the effects of Ru-doped FeNi MOFs on OER activity

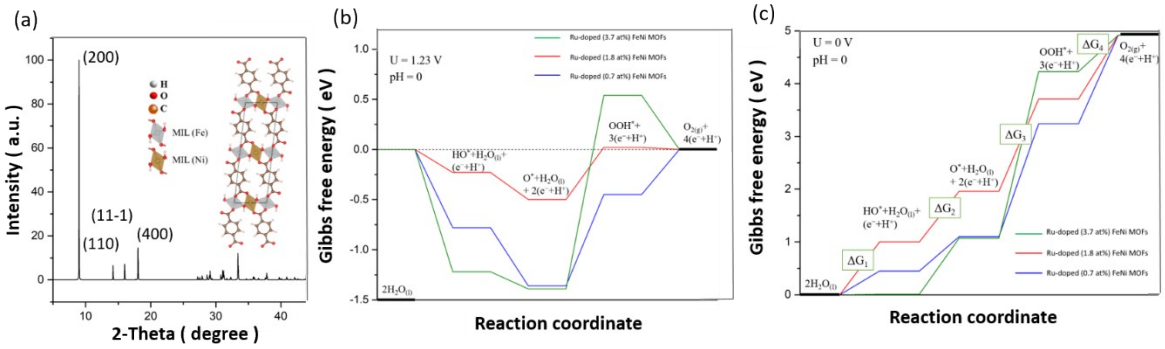

Fig. S6 (a) Illustration of crystallite lattices and correlated diffraction patterns. Estimations of correlated Gibbs free energies for OER processes (b) under U= 1.23 V and (c) under U= 0.00 V.

Fig. S6(a) displays the structural configurations of staggered-FeNi MIL-53 MOF structures according to the experimental results. The overall Gibbs free energies of three Ru-doped FeNi MOFs with various doping concentrations, including 0.7 at%, 1.8 at% and 3.7 at%, under a potential of U= 1.23 V are demonstrated, respectively, as shown in Fig. S6(b). The involvement of OER processes on (200) facet of staggered-FeNi MOF structures is carried out, shown as below,

$$H_2O + * \rightarrow OH^* + H^+ + e^- \quad (1)$$

$$OH^* \rightarrow O^* + H^+ + e^- \quad (2)$$

$$O^* + H_2O \rightarrow OOH^* + H^+ + e^- \quad (3)$$

$$OOH^* \rightarrow O_2 + H^+ + e^- + * \quad (4)$$

In addition, the correlated Gibbs free energy of OER mechanism can be written as follows,

$$\Delta G_1 = G_{OH*} + \frac{1}{2}G_{H2} - G_* - G_{H2O} + qU$$

$$\Delta G_2 = G_{O*} + \frac{1}{2}G_{H2} - G_{OH*} + qU$$

$$\Delta G_3 = G_{OOH*} + \frac{1}{2}G_{H2} - G_{O*} - G_{H2O} + qU$$

$$\Delta G_4 = G_* + \frac{1}{2}G_{H2} + G_{O2*} - G_{OOH*} + qU$$

The thermodynamic overpotential (η_{OER}) of the electrocatalyst is estimated by following formula,

$G_{OER} = max\{\Delta G_1, \Delta G_2, \Delta G_3, \Delta G_4\}$

$\eta_{OER} = G_{OER}/e - 1.23\ V$

Accordingly, the correlated overpotentials are estimated to be 0.91 V, 0.52 V and 1.93 V, with Ru-doping concentrations of 0.7 at%, 1.8 at% and 3.7 at%, respectively. In addition, the estimations of Gibbs free energies at similar (200) lattice plane on the transient occasions of different steps are presented, which indicate the distinct free-energy variations of G_1= 0.45 V (G_1= 0.01 V), G_2= 0.66 V (G_2= 1.06 V), G_3= 2.14 V (G_3= 3.16 V) and G_4= 1.68 V (G_4= 0.69 V) from various Ru-doping concentrations of 0.7 at% and 3.7 at%, respectively, as demonstrated in Figs. 6(c). The results clearly visualize the effect of optimal Ru-doping concentration (1.8 at%) for the improvement of OER activity, as presented in Fig. 4 of main text.

S5 TEM observation and correlated EDS mappings of FeOOH/Ru-FeNi MOFs

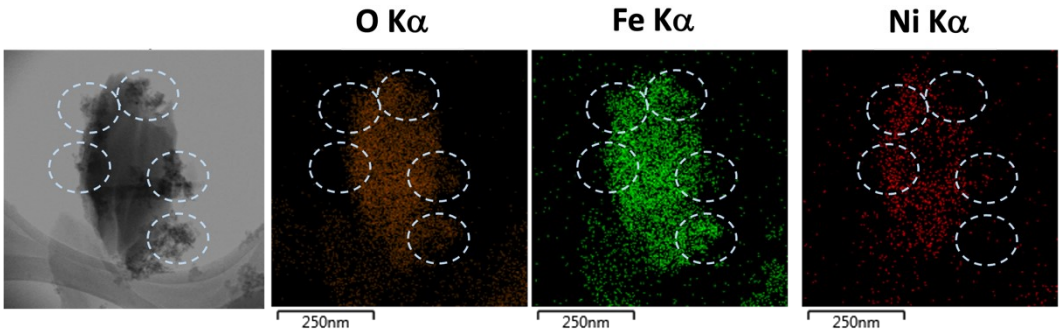

Fig. S7 Large-area EDS mapping of FeOOH/Ru-FeNi MOFs, which evidences the anchoring of FeOOH nanoparticles (denoted as white circles) distributed on MOF surfaces.

S6 Analytic CV measurements of Fe MOFs, Ni MOFs, FeNi MOF, Ru-FeNi MOF and FeOOH/Ru-FeNi MOFs

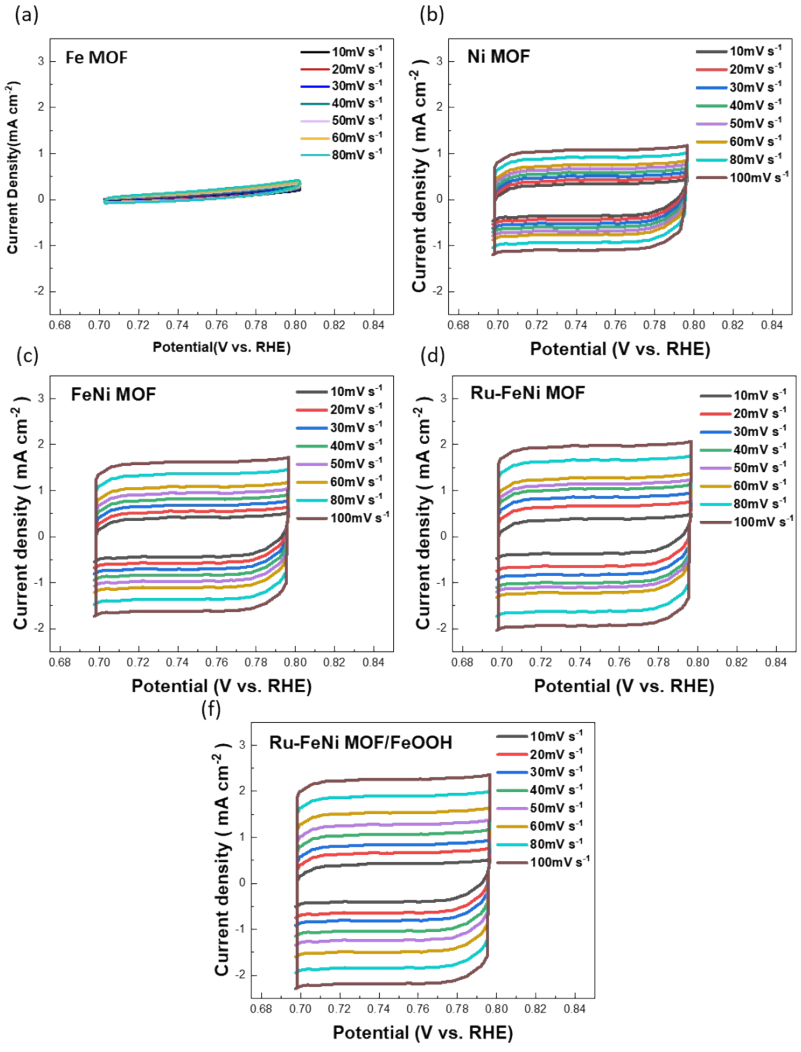

Figure S8 CV plots of (a) Fe MOFs, (b) Ni MOFs, (c) FeNi MOFs, (d) Ru-FeNi MOF and (e) FeOOH/Ru-FeNi MOFs in viewing the current density versus the eemployed potential under different scanning rates (10, 20, 30, 40, 50, 60, 80, and 100 mV s^{-1}), where the magnitudes of C_{dl} are estimated, respectively.

S7 UPS measurement of FeOOH nanoparticles

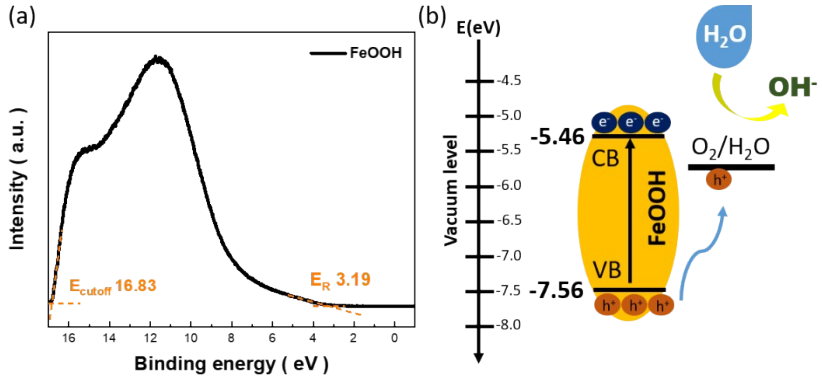

Fig. S9 (a) Measured UPS spectrum of FeOOH nanoparticles. The extracted valence band minimum is estimated to be -7.56 eV. (b) Correlated band diagram when considering the valence-band maximum measured from UPS spectrum and bandgap energy measured from UV/visible absorption spectrum, which clearly indicates that the band alignment between FeOOH/water electrolytes facilitates the hole injection in to electrolytes that initiate OER processes.

S8 Examinations of electrocatalysts after undergoing the OER operation

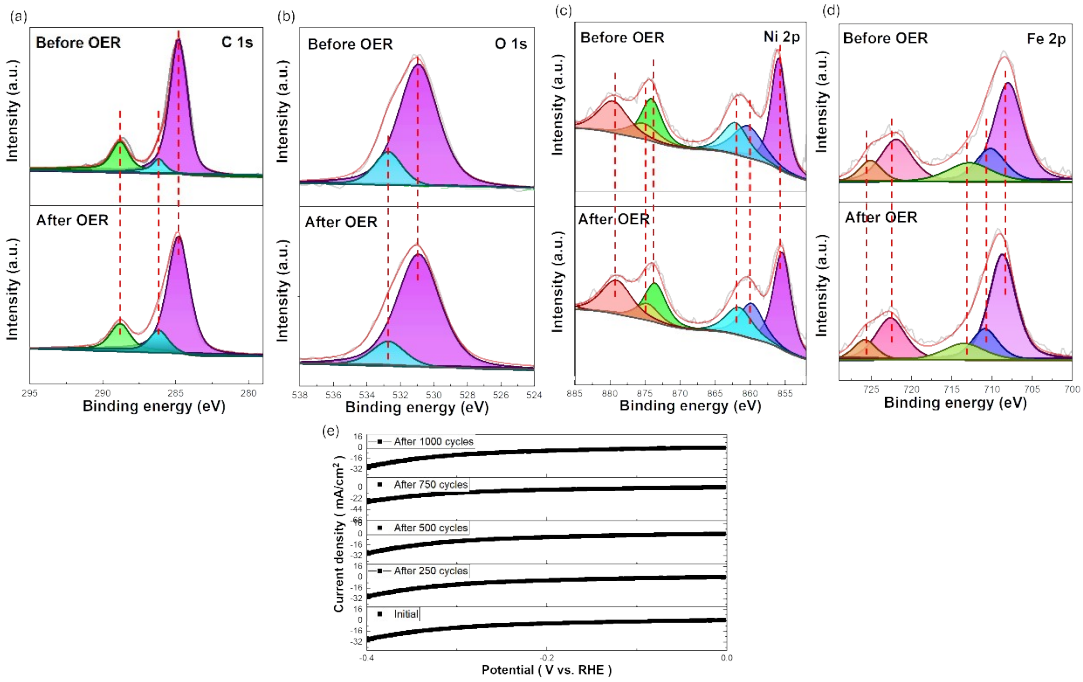

Fig. S10 Spectral examinations of (a) C 1s (b) O 1s (c) Ni 2p (d) Fe 2p in XPS spectra obtained from FeNi MOFs before and after conducting OER operations, respectively, displaying the almost consistent features in comparison with the results prior to OER processes. (e) Comparative LSV curves of catalysts after four various dynamic cycles.

S9 Examinations of HER from FeOOH/Ru-FeNi MOF@NFs

The feasibility of designed heterostructure-based catalysts for HER employment is explored. First, the LSV polarization curves when serving as a cathodic hydrogen evolution catalyst, where the tested catalysts include FeNi MOFs, Ru-FeNi MOFs and FeOOH/Ru-FeNi MOFs, respectively. It is evident that the explicit improvement of the overall current density from FeOOH/Ru-FeNi MOFs due to providing the superior intermediate adsorption/desorption and superior charge-transfer characteristics, as presented in Fig. S11(a). Moreover, the stability of HER performance in FeOOH/Ru-FeNi MOFs, as demonstrated in Fig. S11(b) and S11(c) for cycling and long-term examinations, respectively, exhibits exceptional durability, with minimal decay in current density values of less than 3% after 1000 polarization-curve scans. Notably, the catalyst displays remarkable stability at 100 mA cm^{-2} for over 18000 s, showcasing consistent and sustained performance over extended periods, underlining its promising potentials for durable hydrogen evolution reactions.

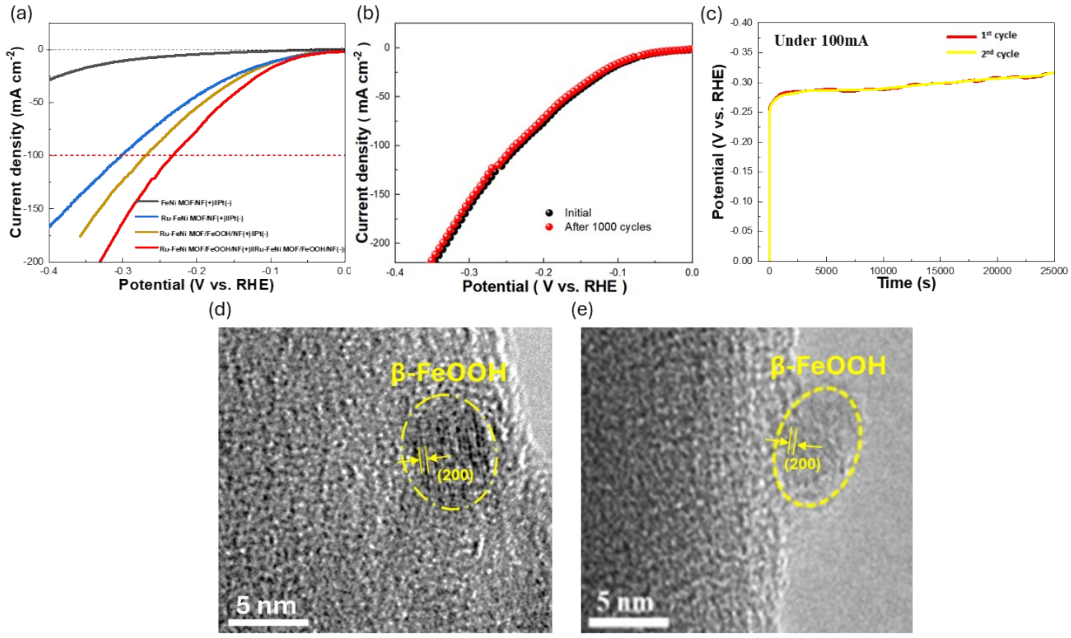

Fig. S11 HER performances of FeOOH/Ru-FeNi MOF@NF based electrocatalysts: (a) LSV results from various catalyst systems. (b) Comparative LSV curves of FeOOH/Ru-

FeNi MOF@NFs before/after 1000 dynamic-cycle scans. (c) Stability test of FeOOH/Ru-FeNi MOF@NFs at current density of 100 mA/cm^2. Representative HRTEM image of FeOOH/Ru-FeNi MOF@NFs (d) before and (e) after 1000 dynamic-cycle scans.

Examinations of Faradaic efficiency are performed under constant current densities of 10 mA cm^{-2} and 100 mA cm^{-2}, with the collection of 4 mL of hydrogen gas per cycle, respectively. After six consecutive cycles at 10 mA cm^{-2} and 100 mA cm^{-2}, respectively, the average time is recorded and summarized in Fig. S12. The calculation of Faradaic efficiency is conducted according to the following formula,

$$\text{Faradaic efficiency } (\xi) = \frac{\alpha F n}{\int_{t1}^{t2} J\,dt} \times 100\ \% \qquad (1)$$

where α the number of electrons involved in the reaction. When calculating hydrogen gas production, α is substituted with 2 in the above equation. F the Faraday constant (96485 C mol^{-1}), n the moles of hydrogen gas produced, t_1 and t_2 the start time and end time of the reaction, and I the magnitude of currents. The resulting Faradaic efficiencies at current densities of 100 mA cm^{-2} and 10 mA cm^{-2} are estimated to be 94.60% and 92.70%, respectively. These results substantiate the excellent electrochemical performance of the synthesized FeOOH/Ru-FeNi MOF based catalysts, displaying the remarkable electrocatalytic efficiencies, as detailed in Fig. S12.

FeOOH/Ru-FeNi MOF@NF (+) ‖ FeOOH/Ru-FeNi MOF@NF (-)

Cycle	1st	2nd	3rd	4th	5th	6th
Time (s)	334	330	336	339	331	329
Mean (s)	333.0					

(Under 100 mA/cm² of current density)

$$\textbf{The Faradaic efficiency } (\xi) = \frac{\alpha F n}{\int_{t1}^{t2} J\,dt} \times 100\ \% = \frac{\textbf{real product}}{\textbf{Theoretical product}}$$

$$= \frac{2 * 96500\ sA/mol * \frac{4.0\ mL}{24500\ mol/mL}}{333.0\ s * 0.1A} \times 100\ \%$$

$$= \mathbf{94.60\%}$$

Cycle	1st	2nd	3rd	4th	5th	6th
Time (s)	3389	3401	3405	3398	3400	3403
Mean (s)	3399.3					

(Under 10 mA/cm² of current density)

$$\textbf{The Faradaic efficiency } (\xi) = \frac{\alpha F n}{\int_{t1}^{t2} J\,dt} \times 100\ \% = \frac{\textbf{real product}}{\textbf{Theoretical product}}$$

$$= \frac{2 * 96500\ sA/mol * \frac{4.0\ mL}{24500\ mol/mL}}{3399.3\ s * 0.1A} \times 100\ \%$$

$$= \mathbf{92.70\%}$$

Fig. S12 Estimations of Faradaic efficiency under the current density of 100 and 10 mA/cm^2, respectively.

S12 Practical assessment for water-splitting tests

The tests are performed with six cycles, where the volumes of H_2 and O_2 generation are separately recorded. The slopes displaying in the correlation between gas volume and time are found to be 2:1, corresponding to the stoichiometric volume ratio of water-splitting expression ($H_2O \rightarrow H_2 + 1/2\ O_2$).

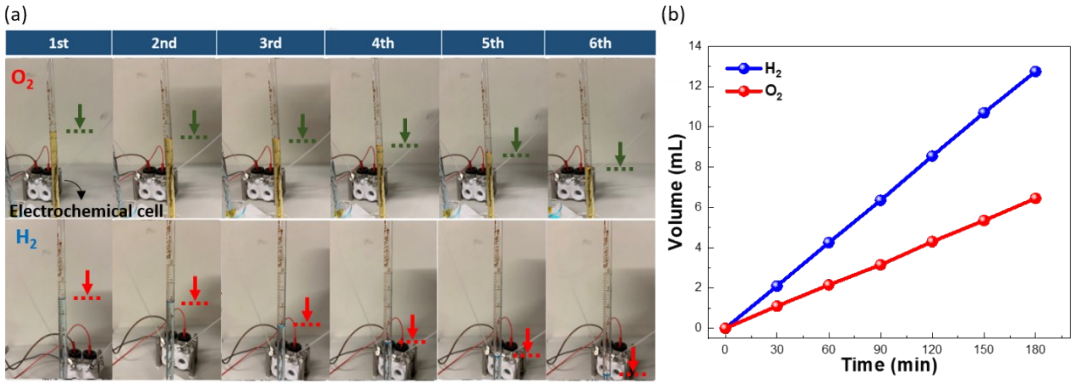

Figure S13 (a) Representative photographs for demonstrating the practical O_2 and H_2 generation in the presence of FeOOH/Ru-FeNi MOF@NFs as unit catalyst system via the standard gas drainage method. The green and red arrows display in the figures denote the interfaces between water and produced gases that allow the quantitative estimation of the gas volume produced via water-splitting reactions, respectively. (b) Evolutions of H_2 and O_2 gases collected by sequential cycles with 30 min as each time interval.

S13 Examinations of turnover frequency from catalysts

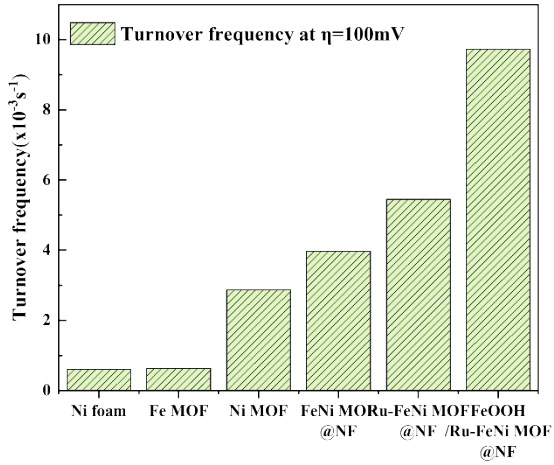

Figure S14 Turnover frequency of FeOOH/Ru-FeNi MOF@NF based electrocatalysts.

Examinations of turnover frequency (TOF) were employed to elucidate the dynamics of intermediate species within the catalytic cycle. By quantifying the frequency at which these intermediates are transformed into final reaction products, TOF offers a deeper understanding of the reaction mechanism and the kinetics involved in intermediate transformations.

TOF can be determined using the formula:

$$TOF = \frac{JA}{4Fm} \tag{2}$$

where J represents the current density under a fixed overpotential (η = 100 mV), A denotes the electrode's surface area (1cm^2), F signifies the Faradaic constant (96485 C mol^{-1}), m indicates the quantity of active sites, and the factor 4 represents the number of electrons needed for the production of one O_2 molecule from water. The quantity of active sites (m) is computed according to the equation:

$$slope = \frac{n^2F^2m}{4RT} \tag{3}$$

Here, the slope is the linear relationship between current density and scan rates. The parameter 'n' symbolizes the electrons transferred, with an assumption of a one-electron process for the oxidation of metal centers in our material (n = 1). Additionally, 'R' and 'T' stand for the ideal gas constant (8.314 J mol^{-1} K^{-1}) and absolute temperature (298 K), respectively. From the TOF results, significant distinctions in the efficiency of intermediate conversion of FeOOH/Ru-FeNi MOF@NF-based electrocatalysts can be

observed. Notably, FeOOH/Ru-FeNi MOF@NFs sample exhibits outstanding TOF values reaching 9.6 $10^{-3}S^{-1}$.

S14 EIS characterizations

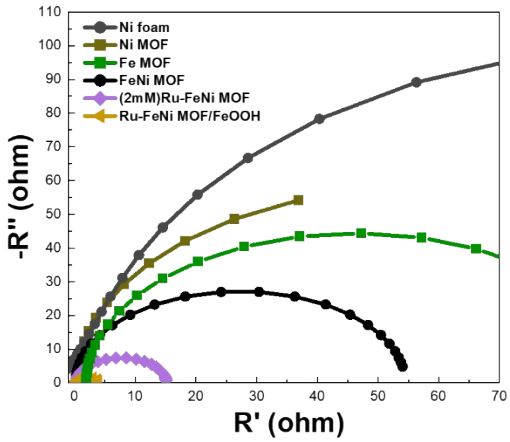

Figure S15 Electrochemical impedance spectroscopy (EIS) spectra of Ni foam, Ni MOF, Fe MOF, FeNi MOF, Ru-FeNi MOF@NFs, and Ru-FeNi MOF/FeOOH, providing comparative insights into the charge transfer resistance and overall electrochemical performance of the various materials.